

EXPERIMENTAL INVESTIGATION OF AN EFFICIENT AND LIGHTWEIGHT DESIGNED COUNTER-ROTATING SHROUDED FAN STAGE

T. Lengyel-Kampmann, J. Karboujian*, G.Charroin*, P.Winkelmann***

*Department of Fan and Compressors, Institute of Propulsion Technology, Cologne, Germany

** Department Component Design and Manufacturing Technologies, Institute of Structures and Design, Stuttgart, Germany

German Aerospace Center

E-Mail: timea.lengyel@dlr.de; jirair.karboujian@dlr.de; guillaume.charroin@dlr.de; peter.winkelmann@dlr.de

ABSTRACT

The German Aerospace Center designed, aero-mechanically optimized and experimental investigated an own counter-rotating shrouded fan stage in the frame of the project CRISPMulti. Their target was on the one hand the generation of a high accurate experimental database for the validation of the modern numerical design and optimization processes, on the other hand the development of a new innovative technology for the manufacturing of the 3D fan blades made of a lightweight CFRP material. The original CRISP-1m test rig designed by the MTU Aero Engines in the 1980th was reused with the new blading for the experimental investigation on the Multistage Two Shaft Compressor Test Facility (M2VP) of the DLR in Cologne.

KEYWORDS

COUNTER-ROTATING FAN, EXPERIMENT, DESIGN, VALIDATION, CFD

NOMENCLATURE

| | |
|-------------|---|
| ADP | Aero Design Point |
| BLR | Boundary Layer Rake |
| CRISP | Counter Rotating Integrated Shrouded Propfan |
| CFRP | Carbon Fiber Reinforced Plastic |
| IPCT | Image Pattern Correlation Technique |
| M2VP | Multistage Two Shaft Compressor Test Facility |
| \dot{m} | Massflow |
| π | Pressure ratio |
| η_{is} | Isentropic efficiency |
| R_k | Recovery factor |
| T | Temperature |
| p | Pressure |

INTRODUCTION

One of the main targets of the engine research is the reduction of the fuel consumption to make the air traffic more environmentally friendly. Therefore, the counter-rotating fan and propeller concepts awakened the interest of the aircraft engine industry due to the opportunity to achieve higher efficiency. The DLR was participating in several international projects dealing with these concepts. Based on this know-how the German Aerospace Center has decided to design an own counter-rotating shrouded fan stage and to test it on the CRISP-1m rig ("Sieber, J. (1991)"). The blade geometry, the blade material and manufacturing technology should be redesigned and significantly improved. Multidisciplinary project targets were striven:

- The main design goal was to maximize the aerodynamic efficiency under restricted static and dynamic mechanical properties of the blade (Görke et al. (2012))
- Engine cycle concept and calculation for an engine with an extremely high bypass ratio
- 30% weight saving (structural weight) with modern CFRP blades
- Development of the automatable manufacturing technology for thermoplastic CFRP fan blades
- The noise emission of the new fan should not be higher than that of a turbofan for engines of the same thrust class. However, a significant noise reduction is not expected and is not realistic based on past experience. The expected goal here is for the CRISPMulti design to have a 6dB lower noise emission than the reference CRISP design.
- Experimental investigations to validate the optimization results, the FE calculational method and the acoustic properties predicted by the DLR in-house code PropNoise

During the design phase an automated multi-objective, multidisciplinary optimization method was applied which allows using simultaneously both a CFD process chain to determine the aerodynamical properties of the fan geometry and also a FE process chain to analyze the structural behavior of the blades and the disc. This FE calculation method of the composite blades is a significant result of the project, which should be validated by the test results.

The instrumentation enables the measurement of the fan aerodynamic by different pressure and temperature rakes and the acoustic measurement by microphones. The unsteady flow field will be characterized by hot wire measurement, optical measurement (PIV) and Kulite measurement.

The experiments on the CRISPMulti rig were extended by inlet distortion measurements in order to investigate the behavior of a Counter Rotating Turbofan under Boundary Layer Ingestion. The boundary layer of the aircraft fuselage ingested into the engine causes a drop in the total pressure in front of the fan. This is generated on the test rig by a distortion grid combined with a honeycomb downstream of the grid to avoid generation of tangential flow velocity components. The design of the distortion grid was carried out as part of the project AGATA and is described in detail in paper "Kajasa et al. (2022)". In order to be able to measure the different circumferential positions in the case of the distorted inlet conditions with all the planned measuring techniques, the inlet distortion itself is rotatable in the circumferential direction. A radial traversing device mounted on the rotatable pipe of the inlet channel enables the continuous and slow introduction of the distortion grid into the inflow channel during operation, controlled from the control room.

The measurement campaign was completed in June 2022. In this paper the experimental SetUp and the results of the stationary measurement will be described in detail. The target of this paper is to present the validation of the numerical performance map of the CRISPMulti rig based on the measured data. The evaluation of the unsteady measurement with inlet distortion will be presented in further publications.

BLADE DESIGN AND OPTIMIZATION

Since the design process of the blades is not the main focus of this paper, only the result of the optimization is presented below. The final blade geometry of the CRISPMulti fan is shown in Figure 1. Since the blades were designed for an existing test rig, some constrains were defined for the design. The exit swirl should be kept close to 0° and the axial Mach number should remain above 0.69 similar to modern aero engines. These constrains and goals are summarized in Table 1.

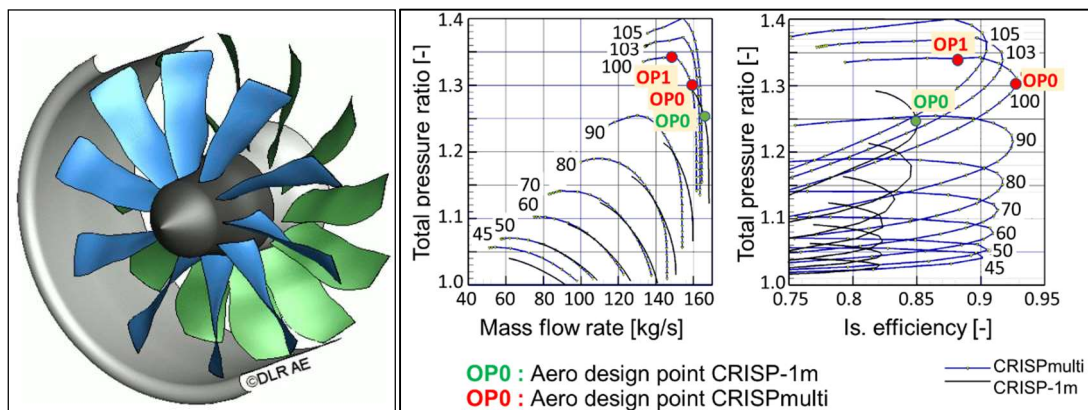


Figure 1 The optimized geometry of the fan stage (left) and the performance map of the optimized geometry compared with the initial design (right)

The optimization objective was defined as maximizing the efficiency and maximizing the stall margin. The rotational speeds and the fan pressure ratio are considered as free parameters in the optimization, so the optimum values are set by the optimization. The resulting values are compared in Table 1 with the initial values from the CRISP-1m fan. It is worth noting that the fan pressure ratio was increased to achieve higher efficiencies. The optimum fan pressure ratio for the counter-rotating fan is at about 1.3. Figure 1 shows the calculated fan map of the optimized CRISPMulti geometry compared with the map of the initial geometry (“Schimming, P. (2003)”).

The final geometry was analyzed by static and dynamic FE simulation in detail.

| Design constrains | | | Design targets | | |
|-------------------|-------------------------------|------|-------------------------|---------|------------|
| Rig constrain | Blade number of Rotor1 | 10 | | CRISP1m | CRISPMulti |
| | Blade number of Rotor2 | 12 | Max. is. efficiency (%) | 87 | 93 |
| | Hub-to-tip ratio | 0,27 | Max. stall margin (%) | 10 | >10 |
| | Outer diameter (m) | 1 | | | |
| Design goal | Tip clearance at R1 @ADP (mm) | 0,65 | Optimisation result | | |
| | Tip clearance at R2 @ADP (mm) | 0,5 | Speed ratio R2 to R1 | 0,86 | 0,79 |
| | Exit swirl @ADP ($^\circ$) | <3 | 100% speed of R1 (RPM) | 4980 | 5044 |
| | Axial Mach number | 0,69 | Fan pressure ratio @ADP | 1,25 | 1,30 |
| | | | Mass flow @ADP (kg/s) | 166 | 159 |

Table 1 Design constrains, targets and the resulted fan parameter

MANUFACTURING AND EXPERIMENTAL VALIDATION OF THE BLADES

The designed blade geometry is provided as a demonstrator for a novel, automatable manufacturing technology for thermoplastic CFRP fan blades, which was developed as part of the Organoblech-CRISP project at DLR. In contrast to the conventional "onion-skin" construction method with individual blanks, the possibility of the thermoplastic base material is used here to

produce the aerodynamic blade geometry by forming a so-called "organosheet" onto the skeletal surface of the blades and subsequently by milling (Figure 2). The design and the manufacturing process are described in detail in the publications "Goerke et al. (2012)" and "Forsthofer et al. (2016)".



Figure 2 Manufacturing process of the CFRP blades (left) and the shaker test (right)

To validate the calculation results, centrifugal tests were carried out on blades for rotor 1 and 2 to determine the static strength. Two Rotor 1 blades were centrifuged in the original installation position, with radial alignment of the blade axis of rotation. Since the test was carried out under vacuum, the bending moments from the pressure load, which compensate for the bending moments from the centrifugal load at the blade root, were missing here. The test was limited to 100% speed (5045 rpm), but due to the missing compensation, the load in the critical root area was 130% of the calculated load. The blades survived the test without damage. One rotor 2 blade was tested to bursting. The blade reached a speed of 6027 rpm (150%) until failure.

The dynamic strength was verified by shaker tests. For this purpose, 5 blades of rotor 1 and 1 blade of rotor 2 were tested on the institute's own shaker (Figure 2). The tip amplitude as the controlled variable of the test was determined for a first test series in such a way that the acceptable dynamic strain amplitude at the CFRP blade/titanium root transition was reached by calculation.

INSTRUMENTATION

Target of the experimental investigation

The aim of the experiment is firstly to verify the optimization result experimentally and secondly to investigate the effects caused at the fan due to boundary layer ingestion. For this purpose, a high-quality experimental database is to be generated, which will be applied to validate the numerical methods. The experimental investigations are carried out in the M2VP test facility in Cologne, at the DLR Institute of Propulsion Technology. Extensive instrumentation is required to fulfill all measurement tasks. Figure 3 shows a schematic overview of all measurement planes.

Standard steady pressure and temperature measurement

In case of the clean inflow, four boundary layer rakes were mounted into the measurement plane E1 to determine the mass flow and the inlet total pressure distribution applying 41 Pitot tubes in the vicinity of the wall (see Figure 4). The distance between the Pitot tubes is higher with increasing distance from the wall: 1.5mm, 3mm, 5mm and 9mm. Hot-wire probes can also be inserted between the boundary layer rakes to determine the flow turbulence quantities at the inlet plane. The same boundary layer rakes can also be inserted in the plane E2b in the circumferential positions 45°; 135°; 225° and 315° in order to be able to determine the mass flow when using the honeycomb.

To determine the total pressure and total temperature distribution downstream of the fan, outlet p_{total} and T_{total} – rakes are used in plane E6 (see Figure 4). Two total temperature rakes with 12 radial

measuring points are used in the circumferential positions 140° and 340° . The measuring points are equipped with pt100 resistance temperature sensors. Two total pressure rakes, each with 12 Pitot tubes and 2 three-hole probes, are used in the circumferential positions 60° and 220° in order to determine the total pressure at the outlet and thus the fan pressure ratio. The static pressure is measured at each measurement plane and along the flow channel at several axial positions by 1mm holes in the casing.

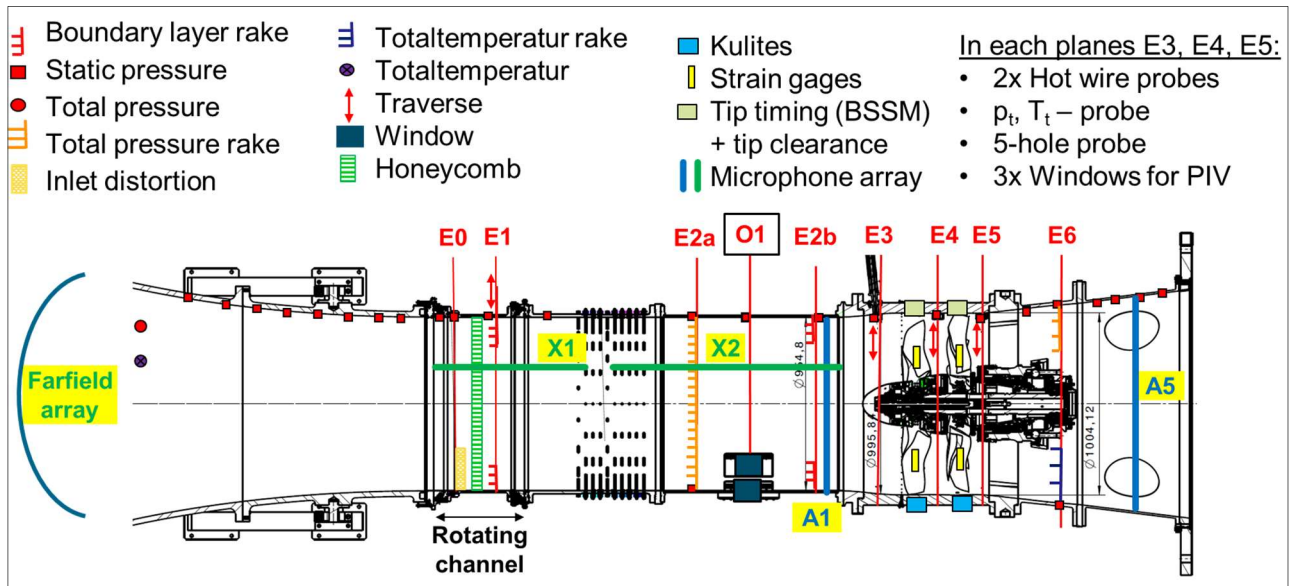


Figure 3 Instrumentation overview

Thus, all in all over 500 pressure measurement points were recorded in the test rig via a PSI measurement unit. The measured temperatures were recorded by a Delphine data acquisition system. All measured values are displayed and stored with a LabView program during the measurement.

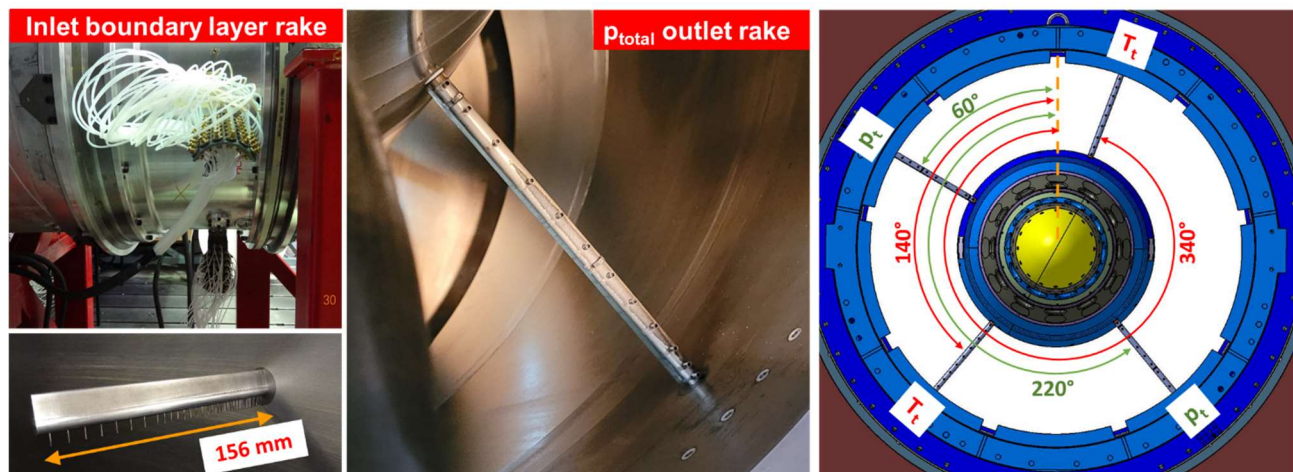


Figure 4 Inlet boundary layer rake (left), outlet total pressure rake (middle) and the circumferential distribution of the four outlet rakes (right)

Inlet distortion with the honeycomb

The pictures on **Figure 5** show the honeycomb with the radial traversing device mounted on the rotatable pipe of the inlet channel. A maximum immersion depth of 140mm is possible. The advantage of this method is, that it allows to apply the distortion only in the stable operating point of the blades. The immersion depth can be controlled and defined afterwards based on the measured effect. In the case of critical blade vibration, the distortion grid can be removed from the channel immediately.

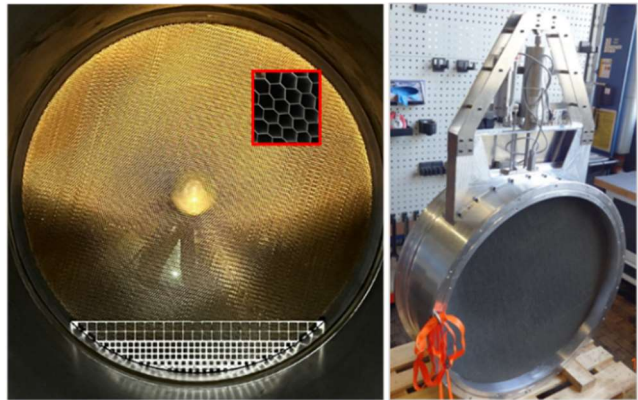


Figure 5 Inlet distortion device

Unsteady measurement technique for the online vibration monitoring

In addition to the measurement techniques presented before, several sensors will be implemented for monitoring the operation of the rig. These all require a high sampling rate to be able to detect the transient phenomena on the rotating components in time. For this purpose, a high-quality data acquisition system from Dewetron DEWEOrion 1624-200 with 160 channels and a maximum sampling rate of 200kHz per channel will be used. Both rotors are provided with an 8-channel telemetry system for signal transmission from the rotating to the stationary system. On rotor 1, it is possible to transmit the bearing temperatures via 8 additional channels on the telemetry.

To monitor the blade deformation, strain gauges are implemented on the pressure side of the blades. The WK-09-375BG-350 from the manufacturer Vishay was selected as a suitable strain gauge for the application on CFRP blades (see Figure 6). The major challenge in using the strain gauges is the positioning and implementation on the blades. Based on the FEM simulation, 4 positions are determined. One blade is instrumented with 2 strain gages. Each strain gage position is used twice, resulting in 8 strain gages per rotor row, distributed over 4 blades.

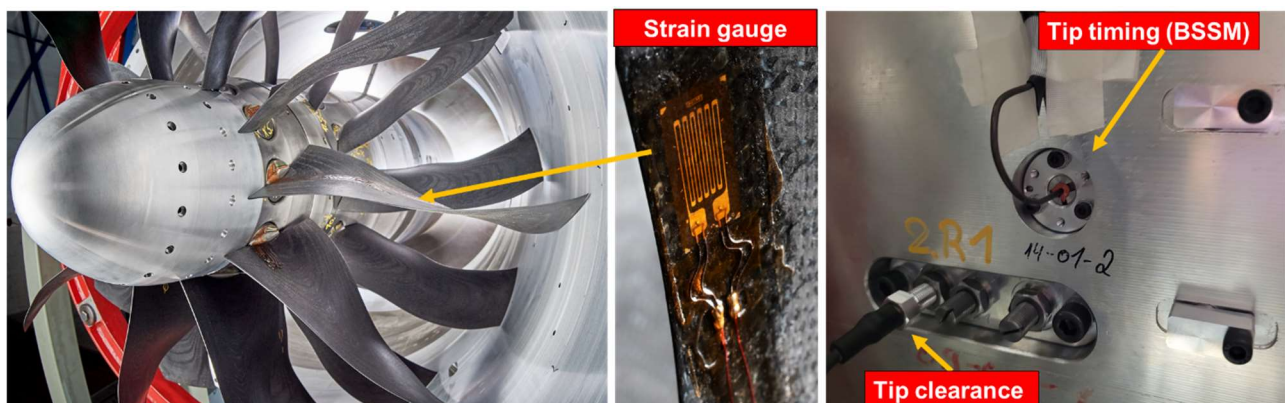


Figure 6 Blade vibration monitoring by strain gauges on the blades (left and middle) and by capacitive sensors in the casing (right)

Further instrumentation for operational monitoring is implemented on the rotor case. DLR's own tip clearance measurement system (Hytron) uses 4 capacitive distance sensors per rotor row (max. 8 channels) to monitor the tip gap during the test. The installation positions in circumferential direction

for both rotors are at 45° , 135° , 225° and 315° . The axial sensor position is determined from the numerical simulations, by finding the position of the minimum tip gap on the fan map. In most cases, these are located at the trailing edge of the blades (see Figure 6).

The entire measurement campaign was supported by tip timing measurement of the MTU Aero Engines (BSSM - Contactless Blade Vibration Measurement System). This measurement method enables not only the tip clearance, but also the blade vibrations to be monitored. A total of 12 capacitive distance sensors are used for this purpose (see Figure 6), which are distributed in the rotor case in two axial positions (2 x 3 pieces) for rotor1 and in one axial position (6 pieces) for rotor2.

The monitoring of the rotor dynamic was performed by spectral analysis of the bearing vibration. For this purpose, as many bearing positions as possible in the rig are equipped with accelerometers (type PCB Synotech). The fixed bearings are monitored in all 3 directions (axial, 2x radial), the floating bearings in 2 radial directions, all in all 20 sensors are mounted in the test rig.

The rotational speeds (RPM) of both rotors are measured by a so-called trigger sensor from the manufacturer Braun GmbH. The sensor is based on the differential Hall effect. A groove or a hole with a certain width and depth is needed in a steel shaft to get a clean square wave signal, from which the rotational frequency can be calculated. A total of 8 sensors are used here for the two shafts: 2 pieces for the 1/rev and 1/blade signals to provide redundancy.

Special aero, structure and acoustic measurement technology

The detailed analysis of the flow field, the blade deformation and the fan acoustic require the application of the special measurement techniques (see Figure 7). IPCT measurements allows the blade deformation measurement under rotating conditions (see in detail by “Willert et al. (2022)”).

The measurement techniques to characterize the flow properties are installed in the rotor case, in the planes E3 - in front of the fan, E4 – interstage and E5 - behind the fan. All 3 planes enable the measurement of the flow velocities by hot-wire anemometry (“Meyer et al. (2022)”) as well as by applying PIV. Flow angles are additionally determined with a 5-hole probe.

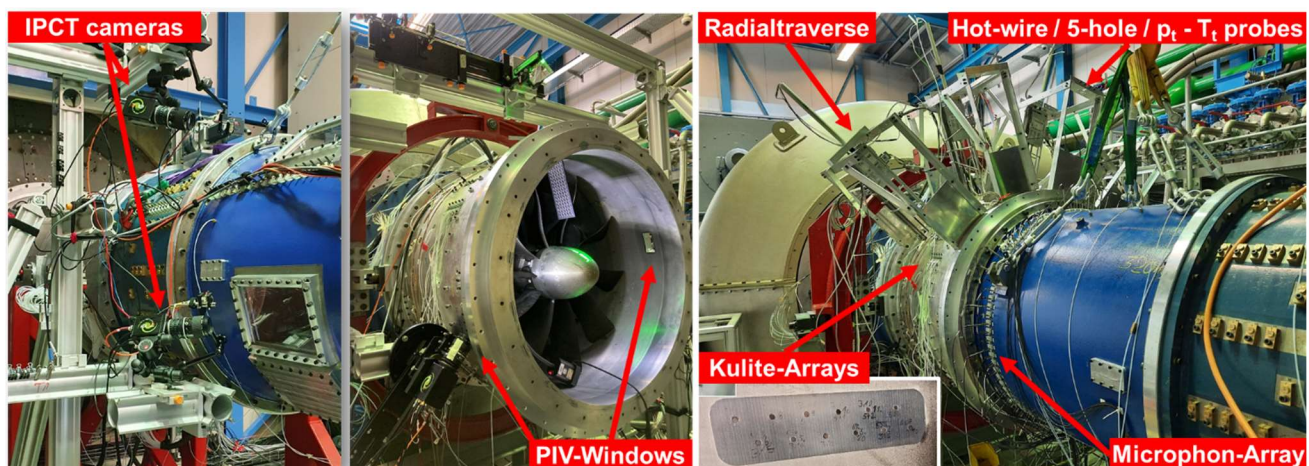


Figure 7 IPCT measurement setup (left), PIV measurement setup (middle) and the configuration for the combined probe-, acoustic- and Kulite-measurement (right)

Kulite array (12 Kulite sensors in one array) is installed above both rotor rows. Several microphone arrays enable the measurement of the acoustic behavior of the fan (detailed in “Meyer et al. (2022)”).

FAN PERFORMANCE MAP MEASUREMENT WITH CLEAN INFLOW

After the commissioning phase, the fan map is measured with the standard instrumentation installed the BLR in the plane E1. Since this plane is located more than 2m upstream from the fan, the pressure losses of the inlet channel are included in the measured pressure ratios, which leads to lower pressure ratio as calculated with the design domain. At the end of the measurement campaign more detailed fan map was measured targeted to achieve the stall margin. In this case the honeycomb was mounted in the plane E1, so the BLRs are installed in the plane E2b. The advantages of this configuration are the more homogeneous inflow and lower channel losses.

Evaluation of the pressure measurement

The inlet total pressure is calculated as the area-weighted averaged value of the radial p_t -distribution measured by the BLRs. The measured mass flow is determined with the following equation for each ring surface:

$$\dot{m} = \rho \cdot V \cdot A = \frac{p}{R \cdot T} \cdot \sqrt{\frac{2}{\kappa - 1} \left(\left(\frac{p_t}{p} \right)^{\frac{\kappa - 1}{\kappa}} - 1 \right)} \cdot \sqrt{\kappa R T} \cdot A \quad (1)$$

where p_t is the total pressure value of the BLRs and p the static pressure measured at the casing in the same plane. The entire mass flow is calculated as the sum of the individual mass flows. Basically, the measured performance map (pressure ratio vs. reduced massflow) is determined only by the pressure measurement with the following equations:

$$\pi = \frac{p_{t,outlet}}{p_{t,inlet}} \quad (2)$$

$$\dot{m}_{red} = \dot{m} \frac{p_{ISA}}{p_{t,inlet}} \sqrt{\frac{T_{t,inlet}}{T_{ISA}}} \quad (3)$$

Where $T_{ISA} = 288,15K$ and $p_{ISA} = 101325Pa$.

Evaluation of the temperature measurement

The temperature measurement is performed by PT100 rakes, which are inserted in the exit flow. Due to the cooling effect of the flow around the Kiel heads, the measured temperature T_{probe} is always lower than the total temperature T_t . Therefore, the application of the recovery factor is necessary to determine the T_t from the following definition:

$$R_k = \frac{T_{probe} - T_s}{T_t - T_s} \quad (4)$$

After the calibration of the recovery factors for all sensor positions at different Mach-numbers the T_s and with this the T_t can be calculated. Error sources like heat conduction through the probe and the Kiel head, and influences of thermal radiation cannot be determined by the calibration.

The isentropic efficiency is determined based on the total pressure and temperature by:

$$\eta_{is} = \frac{\pi^{\frac{\gamma - 1}{\gamma}} - 1}{\tau - 1} \quad (5)$$

With $\tau = \frac{T_{t,outlet}}{T_{t,inlet}}$ and γ the heat capacity ratio for air. Since the uncertainty of the recovery calibration is - depending on the Mach number - relatively high, the error of the efficiency measurement is higher than 1% depending on the Mach number.

The reduced speed N_{red} is defined by the equation:

$$N_{red} = \frac{N}{\sqrt{\frac{T_{t,inlet}^*}{T_{ISA}^*}}} \quad (6)$$

NUMERICAL RANS SIMULATION OF THE RIG TESTS

Numerical Setup

Using a short calculational domain with a course mesh was recommended for the fan blade optimization to accelerate the CFD calculation in the process chain. This flow path is marked with light blue on the Figure 8. On the contrary for the validation the simulated geometry should be as detailed as possible and meshed with high resolution applying a low Reynolds grid ($y^+ < 1$). Therefore, the calculational domain was extended to the measurement planes, E1 or E2b and E6 where the rakes are positioned, see on Figure 8. A commercial mesh generator, AutoGrid5 (developed by NUMECA) was applied to generate the new mesh with hexahedral cells for the validation. Adequate mesh quality was achieved with 3,5 million cells in the entire domain.

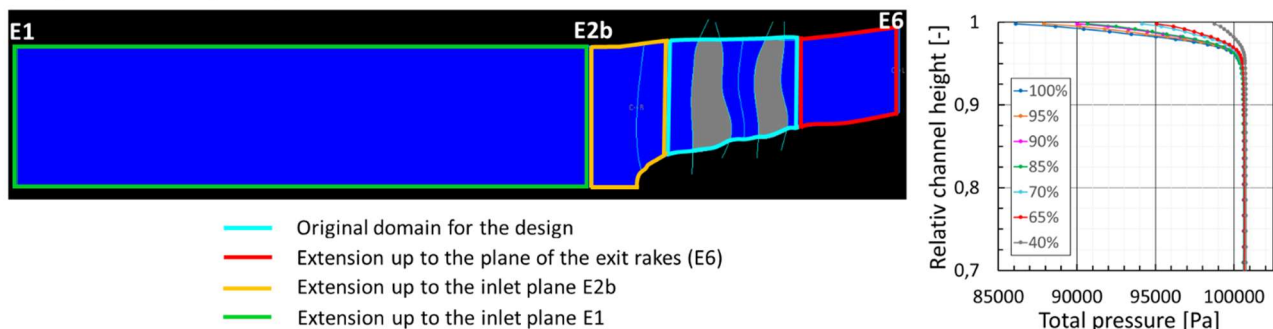


Figure 8 a) Calculation domain for the optimization and for the validation; b) Boundary inlet condition based on the measured results

Boundary conditions

Accurate boundary conditions are very important for the validation of the numerical simulation with the measured data. Accordingly, the measured inlet total pressure with the corresponding boundary layer was applied at the inlet plane for each speed line as 1D radial distribution (Figure 8b). The inlet total temperature was measured in the inlet chamber and kept constant for the speed line. Since the boundary layer is calculated as fully turbulent, the turbulent intensity and length scale has no significant effect on the solution. The inlet flow angle was taken as 0° . The outlet boundary condition was defined by the static pressure as radial equilibrium, changing in small steps to calculate the entire speed line. The real measured speeds for both rotors were taken for the simulation.

RESULTS AND DISCUSSION

The validation results of the CFD calculation based on the fan performance measurement will be presented in this paper. In the first step a numerical parameter study was carried out to examine the effect of the following parameter on the speed line:

1. Sensitivity of the inflow and outflow channel length
2. Tip gap study
3. Sensitivity of the turbulence model

A mesh sensitivity study was carried out as well and concluded that further refinement of the mesh has no effect on the speed line.

Sensitivity of the inflow and outflow channel length

The channel length has a strong influence on both the total pressure ratio and on the isentropic efficiency, since the losses generated through the wall friction are included in both definitions (see

Figure 9). The line colors represent the CFD-calculations with different calculational domains with the corresponding colors on the Figure 8a. More than 1% efficiency is lost (from 92% to 91%) due to the long channel.

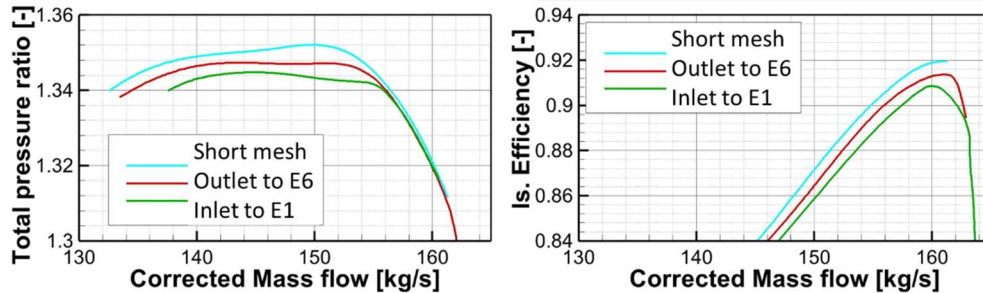


Figure 9 Effect of the considered flow path length on the characteristic (see Fig.8a for colours)

Tip gap study

The study of the tip clearance has a similar effect. The measured tip clearance for Rotor1 and for Rotor2 at 100% speed is about 1.38 mm and 1.67 mm instead of the design gap of 0.65 mm and 0.5 mm. The reason of this high tip gap is the grinding at the abrasive layer in the rotor case during the commissioning phase. Due to the high tip gap the efficiency has lost further 1%.

Sensitivity of the turbulence model

In the last numerical study, the effect of the selected turbulence model was examined. Significant differences can be observed between the Wilcox $k-\omega$ and Menter SST $k-\omega$ models “Menter (1994)” (see Figure 10). The achieved Π_{tot} is much lower (1,5%) than with the Wilcox $k-\omega$ model. The last calculated point on the speed line is near the maximal Π_{tot} with the SST model, so the speed line is shorter and the agreement with the measured speed line (EXP_E1_n100) is much better. The flow field of the last calculated point is plotted with the v_{ax} and TKE-contours on a $x-\theta$ plane at $h_{rel}=0,95$. The separation appears here on the Rotor2, which corresponds with the method to identify the last measured point: the increased vibration on Rotor2 signalized here the separation. The Wilcox $k-\omega$ model appears to be more robust towards separations.

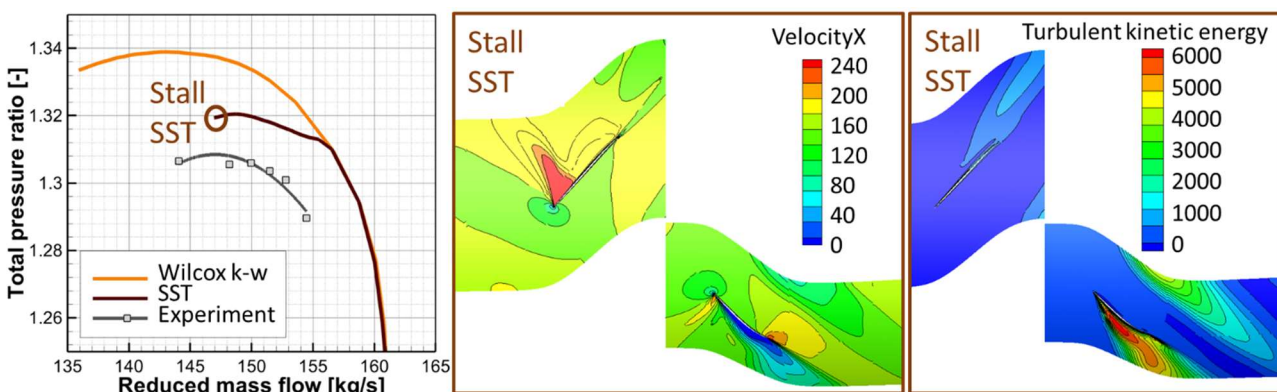


Figure 10 a) Effect of the turbulence model on the speed line, comparison with the measured 100% speed line, b) and c) v_{ax} and TKE-contours in the Stall SST point at $h_{rel} = 0,95$

As conclusion of the numerical studies, we can state that the most suitable numerical setup resulted by applying the Menter SST model with the extended calculational domain and tip gap. However, the performance map with all measured speeds are calculated with both turbulence model

to see the general effects. On Figure 11 the simulation results are plotted by solid lines for the Menter SST model and by dashed lines for the Wilcox $k-\omega$ model. The measured points are shown only with symbols. The different colors mean the different speeds. It can be state, that the optimized ADP was confirmed by the measurement. The maximal deviation in the mass flow is about 1.2%. The possible reason for this could be the uncertainty of the static pressure measurement, if this is not constant in the plane of the BLRs due to the upstream effect of the spinner or other disturbances. The maximal total pressure discrepancies are found at 100% speed. The achieved Π_{tot} is about 0,7% lower as calculated. The explanation for this could be the different geometry or the hub clearance, which will be considered in the detailed evaluation.

The isentropic efficiency is very difficult to determine by temperature measurement for low pressure ratio fans due to the uncertainties of the recovery factor, cooling effect, labyrinth seal, etc. Since the exit rakes are installed in axial direction, the high exit swirl in off-design condition has also an influence on the quality of the measured temperatures. That is why only the results for the high speeds are shown on the diagram. The most reliable efficiency value is the 91,8% at ADP, which is comparable with the calculated 90,7% under test rig conditions.

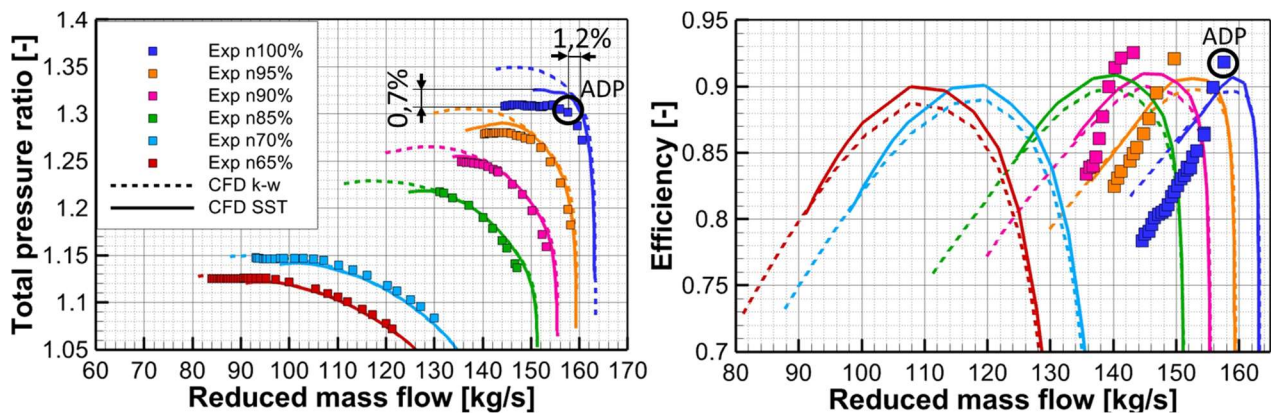


Figure 11 Comparison of the measured and calculated performance maps

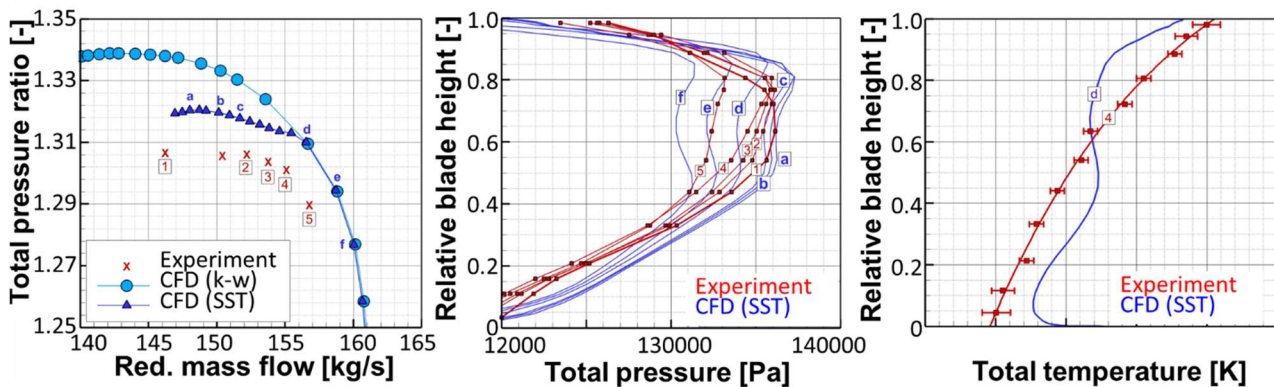


Figure 12 Measured and calculated radial p_t and T_t distributions (100% speed line)

Finally, the measured and calculated radial pressure and temperature distributions are compared on the Figure 12 for the 100% speed and on Figure 13 for the 65% speed. The measured operating points are marked with numbers (1-5) and the simulated points with letters (a to f). A good agreement can be observed between the corresponding points 5-e and 4-d, especially in the gradients of the curves. On the near stall point “1” the pressure is still increased until 70% blade height, but decreased

in the tip region. This indicates the beginning of the separation, which can be seen also in the CFD. The error bars are plotted on the radial temperature distribution to show the higher failure at low speed. Despite the really good agreement between the points “2” and “c” the efficiency cannot be determined correctly.

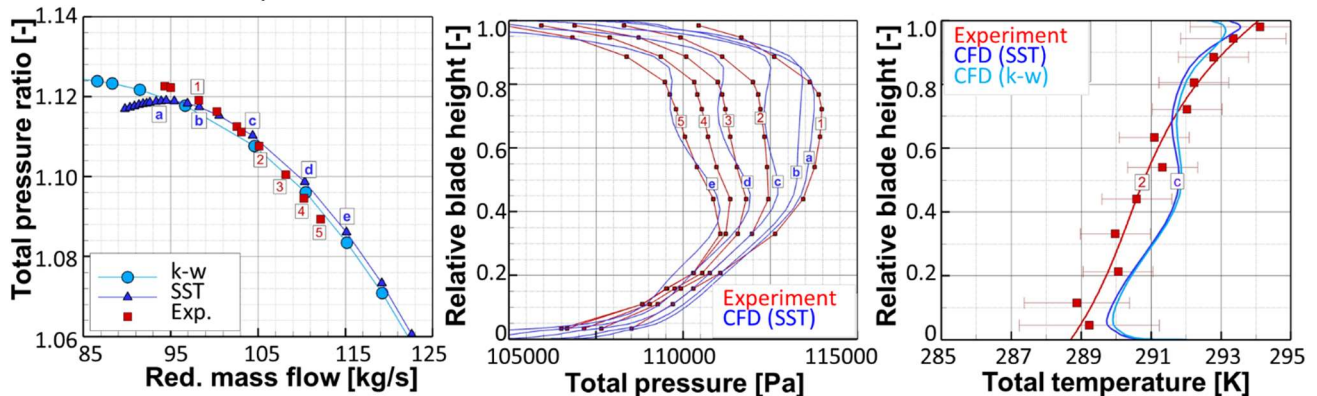


Figure 13 Measured and calculated radial p_t and T_t distributions (65% speed line)

CONCLUSIONS

The experimental investigations on a counter-rotating fan have been presented here. The aim of this paper is to show the validation results of the performance lines of the fan rig based on the measurement. The numerical studies have shown, that the length of the calculation domain, the tip gap height and the selected turbulence model has the most influence on the performance line. Thus, it was confirmed that the objectives of the CRISPMulti project could be achieved. An extensive experimental database was generated for the validation of the numerical methods, which can be evaluated in the future. The effect of the inlet distortion on the fan will be analyzed in detail based on these data in further publications. Not only the aerodynamic properties but the mechanical and aeroelastic design goals of the blades were confirmed through the experimental investigations of the CRISPMulti test rig.

REFERENCES

- Sieber, J. (1991) *Aerodynamic Design and Experimental Verification of an Advanced Counter-Rotating Fan for UHB Engines*. Third European Propulsion Forum, Paris, France
- Schimming, P. (2003) *Counter Rotating Fans — An Aircraft Propulsion for the Future?* Journal of Thermal Science, Vol. 12, No. 2, pp. 97–103. <https://doi.org/10.1007/s11630-003-0049-1>
- Goerke, D., Le Denmat, A.-L., Schmidt, T., Kocian, F., and Nicke, E. *Aerodynamic and Mechanical Optimization of CF/PEEK Blades of a Counter Rotating Fan*. Denmark, 2012.
- Kajasa, B., Lengyel-Kampmann, T., Meyer, R. (2022) *Numerical and Experimental Design of a radial displaceable Inlet Distortion Device*, ISABE, Ottawa
- Forsthofer, N., and Reiber, C. *Structural Mechanic and Aeroelastic Approach for Design and Simulation of CFRP Fan Blades*. 2016
- Menter, F.R. *Two-equation eddy-viscosity turbulence models for engineering applications*. AIAA J., 32(8):1598–1605, August 1994
- Willert, C., Klinner, J., Schroll, M., and Lengyel-Kampmann, T. “*Measurement of Aerodynamically Induced Blade Distortion on a Shrouded Counter-Rotating Prop-Fan*.” 2022, p. 5
- Meyer, R., Tapken, U., Klähn, L., Behn, M., Rudolphi, A., *Experimentelle Untersuchung der Auswirkung von Grenzschichteinsaugung auf die Zuströmturbulenz und die Aeroakustik des gegenläufigen Fan-Modells CRISPMulti*, DLRK, Dresden 2022